Time frequency analysis for the evaluation of ignition delay in conventional and PCCI combustion modes

AUTHORS: d'Ambrosio S (*), Ferrari A and Mancarella A
Energy Department, Politecnico di Torino, Corso Duca degli Abruzzi 24, 10129, Italy
(*) Corresponding author. E-mail: stefano.dambrosio@polito.it. Phone: +390110904415

Time frequency Analysis for the Evaluation of Ignition Delay in Conventional and PCCI Combustion Modes

Abstract

In-cylinder pressure signal has been widely adopted to obtain simple offline and online diagnosis of the combustion process through one-zone analysis, which provides the apparent heat release of the mixture. The present paper also starts from the in-cylinder pressure measurement to apply time frequency analysis for an alternative evaluation of the combustion events. A comparison with traditional one-zone analysis is then performed. In particular, time frequency analysis is here applied for the investigation of all the characteristic events that define the fuel ignition delay, i.e. hydraulic start of injection, first, along with the corresponding start of combustion, next. The study here reported is relative to single-injection patterns and has been applied to both conventional and premixed low-temperature diesel combustion modes. For the considered injection pattern, time frequency analysis, compared to single-zone combustion model supplemented by measurements of injection rate at the hydraulic rig and by engine measurements of fuel injection pressure in the injector supply pipe, provided precise evaluation of the relevant combustion events.

Keywords: ignition delay, time frequency analysis, ignition dwell, start of combustion, diesel combustion.

Highlights

The time frequency analysis can detect both start of injection and start of combustion.
The time frequency analysis can provide the evaluation of ignition delay in diesel engines.
The time frequency analysis is applicable to both conventional and innovative diesel combustion modes.

1. Introduction

In a diesel engine, one common definition of ignition delay (ID) is the elapsed time from the hydraulic start of injection (SOI_h), i.e. the instant of time at which the fuel is effectively delivered into the combustion chamber, to the following start of combustion (SOC) [1,2], when the air-fuel mixture has just reached its autoignition temperature [3]. Besides this rather simple definition, an accurate ID estimation can be an issue, since SOI_h and SOC timings (in terms of crank position) are not directly available.

A measurement that is generally simple to carry out at the engine test rig is the timing of the electrical command sent to open the injector needle, i.e. the electric start of injection (SOI_e). However, there is always a temporal delay between this SOI_e and the actual SOI_h [4], whose estimation (potentially for every injection pulse) also needs further experimental data (from a hydraulic rig) that provide the injector nozzle opening delays (NOD), usually reported as a function of nominal rail pressure (p_{rail}) and energizing time (ET) [5].

A proper definition of SOC is substantially harder to find [6,7] and several criteria can be used to quantify it. One is through the "difference pressure" approach, whereby the SOC is detected based on the difference in temporal evolution between combustion and motored in-cylinder pressure (p_{cyl}) traces. In particular, the SOC would be determined as the specific crankshaft angle (°CA) at which the deviation of the combustion pressure curve from the motored one goes beyond a defined threshold [5,8,9,10]. Other methods for SOC determination rely on the rate of in-cylinder pressure rise [11], by evaluating either the first [12], the second [13] or the third [14] derivative of p_{cyl} with respect to °CA [7,15]. The SOC may then be defined as the time instant at which the considered derivative of the pressure either raises sharply or reaches a maximum with respect to °CA.

Several other methods for SOC estimation employ the net (also called apparent) HRR, which accounts for two different contributions: the whole heat released by the combustion process (referred to as gross heat release) and the heat transfer taking place from/to the in-cylinder gases through the walls surrounding the combustion chamber. Ultimately, considering that the predominant direction of this aforementioned heat transfer is towards the walls, the cumulative net heat release results to be smaller than the gross heat release, generally by about 20% [1]. SOC-estimation methods built on the net HRR are commonly used, because the net HRR evaluation is considered reliable and simple to calculate [1]. To identify the SOC, these methods pinpoint the °CA at which the first fraction of chemical energy from combustion starts being released [5,16,17,18]. Its detection would then be associated to the time at which the net HRR reaches its negative minimum (due to fuel heating and vaporization), returns to zero [2,19,20] or reaches a fixed amount of the total heat released [20], e.g. 2 J/°CA [21]. The computation of the SOC can also be similarly performed out of the gross heat release, with little to no variations (within experimental uncertainty) [21]. Nevertheless, it is more convenient to directly exploit the net HRR, which can be determined straightforwardly (i.e., without the need of any heat transfer model [1]) just from the experimental in-cylinder pressure signal, by applying either one-zone (also called single-zone) [22] or two-zone (also called double-zone) thermodynamic models [23]. The HRR-based method can also be adopted for multiple injections: in this case, the SOC of the following injection events can be distinguished by identifying the local minimum points along the HRR curve.

Other criterions to identify the SOC may be based on flame luminosity, but they are hardly privileged over the above-mentioned pressure-based approaches, since they generally enhance the potential for error. The reason for this is that the first detection of the flame inside the combustion chamber commonly happens after the first increase in pressure [1].

It is generally agreed that the heavy dependency of ID on temperature (T) can be expressed through a proper Arrhenius-type correlation [2,3,4,5,12,24,25]. In particular, many of the proposed ID correlations have been based on the values of in-cylinder pressure and temperature [1,13,26,27]. However, for some fuels, which exhibit cool flames, the ID cannot be expressed by means of a single Arrhenius equation in the whole temperature domain, since an intermediate temperature range exists in which ID can change very little or even increase with increasing temperature. This phenomenon is usually referred to as negative-temperature coefficient (NTC) behavior [3]. For those fuels that show NTC behavior, plots of ID in a logarithmic scale versus $1/T$ can be divided into three subdomains: high-temperature (HT) (usually above 1000 K), low-temperature (LT) (usually below 650 K) and NTC in between [28,29].

When the combustion process is characterized by a two-stage ignition, a crucial role is played by the first-stage, since the following second-stage ignition is heavily affected by the intermediate chemical species and the heat release produced by the cool flames [30]. In the event of a two-stage combustion, it is worthwhile defining two parameters that characterize the whole ignition process [31,32,33]: the start of combustion of the cool flames SOC_{cool} (i.e., the time instant that marks the beginning of the LT combustion) and start of combustion of the hot flames SOC_{hot} (i.e., the time instant that marks the beginning of the HT combustion). Therefore, more parameters related to the ignition delay exist: $ID_{cool} = SOC_{cool} - SOI_h$, $ID_{hot} = SOC_{hot} - SOC_{cool}$ and a total or overall ignition delay, namely $ID_{tot} = SOC_{hot} - SOI_h = ID_{cool} + ID_{hot}$

The comparison between these ignition delays for the diesel spray indicates that while both ID_{cool} and ID_{hot} shorten as SOI_e is delayed, this effect is more evident on ID_{cool}, suggesting that the initial T has a major impact on ID_{cool}. As in-cylinder pressure increases, both ID_{cool} and ID_{tot} decrease, and this shrinks the NTC region [34], which eventually disappears above a certain pressure threshold.

In low temperature combustion (LTC) systems, the fuel exhibits an ignition delay much longer than what is typically encountered in conventional diesel combustion. The correlation between SOI_h and SOC is usually weaker and combustion control becomes more challenging. The longer ID provides more time for fuel vaporization, hence more homogeneous air-fuel mixture. The higher premixing favorably affects PM emissions and the higher homogeneity results in more uniform and lower temperature across the combustion chamber [35], thus reducing the thermal formation of NO_x emissions.

LTC ignitions can occur in either single or two stages. Fuels featuring two-stage ignition were shown to offer great benefits as far as combustion phasing and LTC operation range extension are concerned [36,37]. While LT reactions are not a strict requirement for successful premixed LTC operation, they can have a significant impact on the HT reactions

and need to be accounted for [3]. In conclusion, a precise ID estimation to carefully control combustion phasing is even more important in LTC than in conventional combustion mode.

In the present paper, the combustion pressure signal has been investigated through the theory of time frequency analysis (TFA), for a single injection strategy at part loads under premixed charge compression ignition (PCCI) combustion and at a full load under conventional diesel combustion, with the aim of detecting significant events. The results of the TFA, which were compared to standard apparent one-zone heat release rate analysis (for SOC estimation) coupled with further dedicated experimental data (for SOI_h estimation), proved to be able to provide accurate evaluation of SOC as well as SOI_h, both in one-stage and two-stage combustion modes, thus confirming to be a reliable tool in the evaluation of ignition delays. This preliminary analysis of the ID calculation through the TFA was applied to simple single-injection strategies to evaluate the possibility of capturing combustion events. The next step in future activities will be the application of the same analysis to more complex injection trains featuring multiple injection shots.

2. Experimental setup

The experimental results are part of a purposely dedicated experimental test campaign that has been performed at the Politecnico di Torino, at the dynamic engine testbed of the Internal Combustion Engines Advanced Laboratory. Two engines, derived from the same baseline hardware, have been considered for the experimental tests of this investigation. Both of them were provided by FPT Industrial: the first is a conventional version, mass-production F1C engine, homologated as EURO VI (hereinafter referred to as F1C Euro VI), the second is an innovative version that has been suitably optimized to work under PCCI combustion mode (hereinafter referred to as F1C PCCI). Their main technical specifications are listed in Table 1, while Fig. 1 shows a schematic of their installation at the testbed (the engine layout and the measurement equipment are basically the same for the two engines).

Table 1. Comparison of the main technical specifications of the conventional F1C Euro VI and of the PCCI version of the engine.

Engine type	FPT F1C Euro VI	FPT F1C PCCI
Number of cylinders	4	
Displacement	2998 cm^3	
Bore / stroke	95.8 mm / 104 mm	
Rod length	160 mm	
Compression ratio	17.5 : 1	14.6 : 1
Valves per cylinder	4	
Turbocharger	Single-stage VGT	Single-stage VGT (smaller turbine compared to the F1C Euro VI)
Fuel injection system	Common rail injection system	
Injector static flowrate	990 cm^3 in 30 s at 100 bar upstream pressure	750 cm^3 in 30 s at 100 bar upstream pressure
Injector cone angle	139.8°	130°
EGR circuit type	Short-route, high pressure, cooled	
EGR cooler	Max thermal power: 6kW	Max thermal power: 32kW

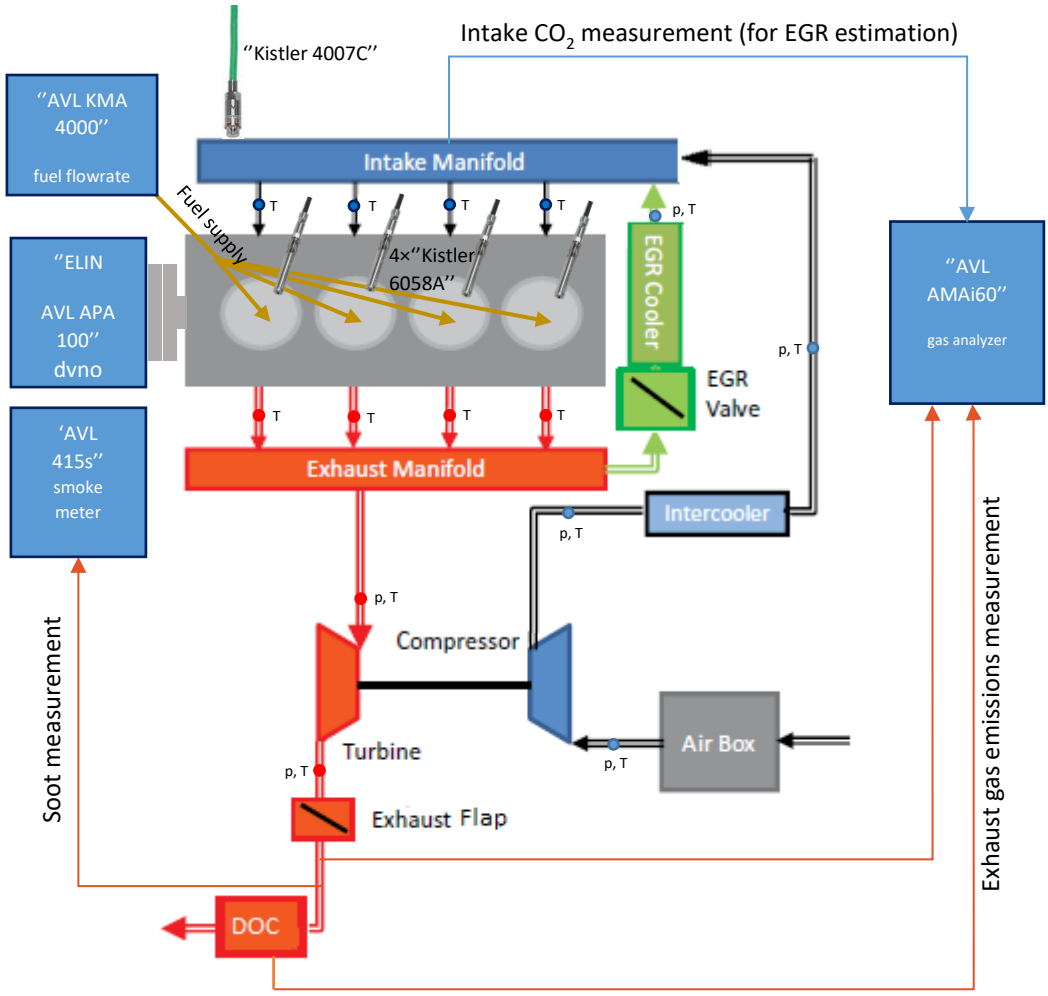

Figure 1. Schematic of the F1C PCCI engine installed on the dynamic testbed at the Politecnico di Torino.

Both engines, fueled with the same conventional diesel oil (EN 590), are equipped with high-pressure (short-route) cooled EGR systems, with a cooled EGR valve located upstream of an EGR cooler. Given that in the PCCI version a higher EGR flow rate is needed, the conventional high-pressure EGR system (featuring a poppet EGR valve and a cooler with 6 kW of maximum thermal power) was replaced by a system with EGR throttle valve and a cooler with 32 kW of maximum thermal power (derived from heavy-duty commercial vehicles). Other differences between the two engine versions encompass piston geometry and compression ratio, turbocharger group and injector flow rate [8]. Low-frequency pressure and temperature measurements were performed for both engines in several points of the air, EGR and exhaust flow paths for a complete monitoring of engine parameters. In addition to this, high-frequency in-cylinder pressure measurements (every 0.1 °CA) were performed in the four cylinders of both engines through Kistler 6058A piezoelectric transducers. Their in-cylinder signals were referenced by an absolute pressure sensor, namely a Kistler 4007C piezoresistive transducer, fitted in the intake manifold.

The testbench also included an AVL KMA4000 fuel flow-rate meter and an AVL AMAi60 exhaust gas analyzer, composed of two trains endowed with suitable measurement devices able to determine the concentrations of NO_x/NO,

HC, CH_4, CO, CO_2 and O_2 both upstream and downstream of the aftertreatment system. An additional line, equipped only with a CO_2 infrared detector, is employed to compute an estimation of the EGR rate. To measure soot emissions under steady state conditions, an AVL 415S smoke-meter is available. The automation software, used to control all the above-mentioned measurement equipment, is AVL PUMA Open 1.3.2, while IndiCom and AVL CONCERTO 5 were used, respectively, for indicating measurements and data postprocessing.

Previous works [38] have estimated that the expanded uncertainty on the measurements of exhaust pollutant emission concentrations carried out at this engine testbed lies in the range of 2 to 4%. Then, to estimate the extended uncertainty on brake specific emissions, also the AVL KMA accuracy (0.1% over a fuel flowrate range of 0.28 to 110 kg/h) and the maximum error on engine speed (1.50 rpm at full scale) and torque (0.30 Nm at full scale) measurements need to be considered.

The hydraulic tests, discussed in this paper, have been conducted at a hydraulic test rig [39] endowed with purposely dedicated devices to evaluate the fuel injected volume, mass and instantaneous flowrate, the fuel pressure signal within the pipe that joins the rail to one of the injectors as well as the electrical current signals sent to the injector command system. In particular, the instantaneous injection rate and the injected mass were evaluated through an HDA flowmeter, while the fuel pressure time history at the injector inlet was measured by a piezoresistive transducer. The working fluid was ISO-4113 oil [40,41], employed as a diesel-like surrogate liquid owing to its ability to properly simulate its properties at low temperatures (up to 120°C).

More details about the engine and the test benches can be found in [8,42].

3. Time frequency analysis (TFA)

First, the experimental in-cylinder pressure signal, namely $p_{cyl}(t)$, has been divided into shorter temporal segments through a windowing operation realized by means of a mobile Hann function, $h(t-\tau)$, where τ represents a parameter that corresponds to the center of the window time length. Then, a Short Time Fourier Transform, which is defined as follows, has been applied:

$$\hat{F}_l(\omega,\tau) = \int_{-\infty}^{+\infty} p_{cyl}(t)\, h(t-\tau)\, e^{-j\omega t} dt \tag{1}$$

where ω is the circular frequency and j is the imaginary unit.

Shifting the center of the Hann window in Eq. (1) along the time domain is possible by varying τ by finite steps of amplitude $\Delta\tau$, thus obtaining different local Fourier spectra. The wider the overlap period (in the time domain) between two consecutive positions τ_i and $\tau_{i+1}=\tau_i+\Delta\tau$ of the Hann window h, the more gradually the resulting Fourier spectrum will vary with respect to time [43].

The square modulus of $\hat{F}_l(\omega,\tau)$ represents the spectrogram $P_{sp}(t,v)$, which has been selected as the time-frequency distribution in the developed code:

$$P_{sp}(t,v)=\left[\int_{-\infty}^{+\infty} p_{cyl}(\tau)\,h(\tau-t)\,e^{-j2\pi v\tau}d\tau\right]^2=\hat{F}_l(\omega,\tau)^2 \tag{2}$$

The time-frequency distribution can be interpreted as a density probability function and has been employed in the simulation code to calculate the mean instantaneous frequency (MIF) $\bar{v}(t)$, as shown by the following formula [43]:

$$\bar{v}(t)=\frac{1}{\int_{-\infty}^{+\infty}P_f(t,v)\,dv}\int_{-\infty}^{+\infty}v\,P_f(t,v)\,dv \tag{3}$$

Eq. (3), which represents an essential relation for many different engineering applications, gives the baseline harmonic contribution to the signal $p_{cyl}(t)$ at every time instant. Further details about the time frequency analysis are reported in [43]. In the present paper, the mean instantaneous frequency is applied to determine the ignition delay.

4. Results and Discussion

The TFA has been applied to working conditions characterized by a single injection strategy in order to check its potentialities in evaluating the combustion dynamics and in particular the ignition delay. Single injection calibrations can effectively be applied to a narrow area at high load and speed in conventional diesel engines, whereas they can be adopted in a wider portion of the engine map at low load and speed in PCCI engines.

Figures 2-5 refer to four distinct engine key points: the single injection pattern was applied to both the F1C PCCI (Figs. 2-4, part load) and the F1C Euro VI (Fig. 5, full load) engines. Figs. 2-4 correspond to similar engine part load operating conditions, in terms of engine speed *N* [rpm] and *bmep* [bar]; the differences are mainly related to the inducted air quantity per cycle and to the injection timing.

The input parameters of the key points have been detailed in Table 2: these are the engine speed (*N*), the energizing time (*ET*) of the injection pulse, the electric start of injection (SOI_e), the nominal rail pressure (p_{rail}) and the air quantity that determines the EGR fraction (and hence the air-fuel ratio λ).

Table 2. Engine working conditions for Figs. 2-5.

Figure	Engine	Input parameters					Measured Values		
		N [rpm]	SOI_e [°CA bTDC]	ET [μs]	p_{rail} [bar]	*Air* [mg/stk]	x_{EGR} [%]	λ [-]	*bmep* [bar]
2	F1C PCCI	2000	22	400	1000	370	55	1.42	3.3

3	F1C PCCI	2000	22	400	1000	544	41	2.07	3.4
4	F1C PCCI	2000	28	400	1000	370	55	1.41	3.4
5	F1C Euro VI	3500	13	587	1800	1393	0	1.59	14.2

In the upper part of each diagram of Figs. 2-5, the in-cylinder pressure (p_{cyl}), the electric current to the solenoid injector and the fuel pressure time history within the pipe that joins the rail to the inlet of one of the injectors ($p_{inj,in}$) have been plotted. Furthermore, the experimental injected flow-rate, captured using the HDA flowmeter at the hydraulic test rig for the same p_{rail} and ET values as for the tests on the engine, has been reported. The bottom part of each figure reports the results of single-zone analysis, performed with the software AVL CONCERTO, in terms of instantaneous net heat release rate (HRR) and burned mass fraction (x_b); moreover, the instantaneous value of the mean frequency $\overline{\nu}$ has been plotted. The MIF was applied to the Δp_{comb} signal, which roughly represents the p_{cyl} portion that should have the closer relation to the combustion events [43]. Indeed, the in-cylinder pressure can be considered as the sum of a mechanical part (motored pressure p_{mot}), which determines compression and expansion phases and considers the effect of piston motion, and of a combustion part (combustion pressure Δp_{comb}) that arises because of exothermic reactions of the fuel with air:

$$p_{cyl} = p_{mot} + \Delta p_{comb}$$

Therefore, the application of TFA to Δp_{comb} avoids that larger pressure variation due to piston motion can mask minor pressure variation due to combustion events (for instance related to fuel injection and evaporation).

The motored pressure is here calculated based on the firing pressure (p_{cyl}) trace, by considering an appropriate polytropic compression coefficient, which is evaluated over a crankshaft angle interval that spreads out from the beginning to the end of the compression phase. In fact, in a turbocharged engine a real motored cycle acquisition could not take into account the boost pressure provided by the turbocharger. In the present activity, as the value 360 °CA corresponds to the TDC of combustion, the start of compression is fixed at 280 °CA, that is, an angular position at which the intake valves are already closed and compression has already started. The compression phase is conventionally considered as ended at the crank angle at which the electrical current to the injector starts to become higher than zero, and it can therefore vary according to the considered SOI_e value.

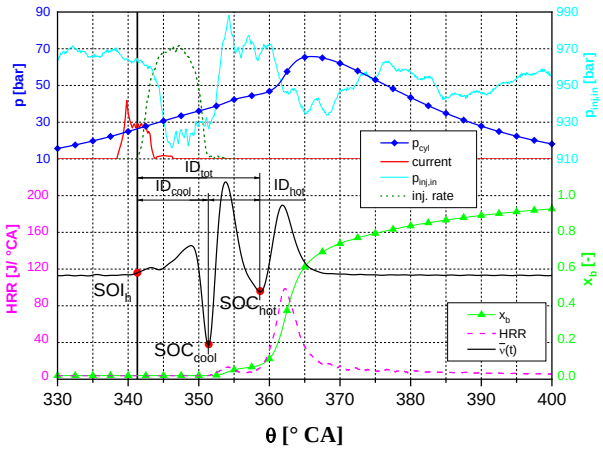

Figure 2. Experimental data (upper part) and calculated parameters (lower part) for the working conditions 1 in Table 2 (F1C PCCI, 2000 rpm × 3.3 bar, SOI_e = 22° bTDC, ET = 400 µs, p_{rail} = 1000 bar, *Air* = 370 mg/stk, x_{EGR} = 55%).

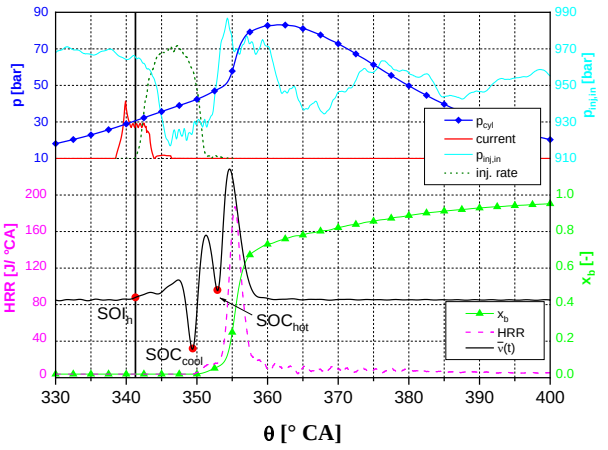

Figure 3. Experimental data (upper part) and calculated parameters (lower part) for the working conditions 2 in Table 2 (F1C PCCI, 2000 rpm × 3.4 bar, SOI_e = 22° bTDC, ET = 400 µs, p_{rail} = 1000 bar, *Air* = 544 mg/stk, x_{EGR} = 41%).

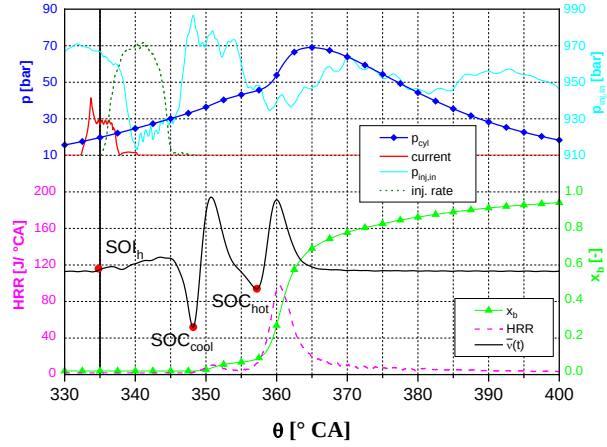

Figure 4. Experimental data (upper part) and calculated parameters (lower part) for the working conditions 3 in Table 2 (F1C PCCI, 2000 rpm × 3.4 bar, SOI_e = 28° bTDC, ET = 400 µs, p_{rail} = 1000 bar, *Air* = 370 mg/stk, x_{EGR} = 55%).

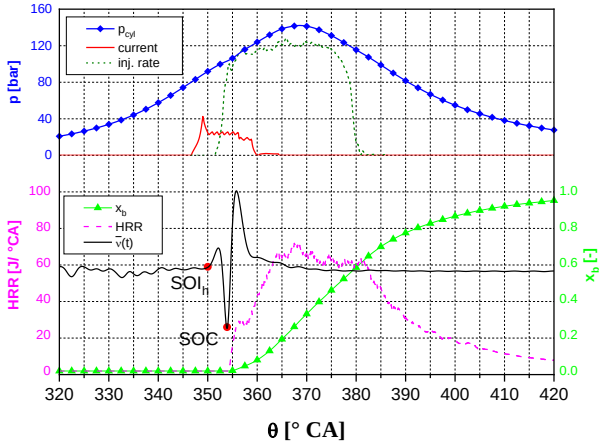

Figure 5. Experimental data (upper part) and calculated parameters (lower part) for the working conditions 4 in Table 2 (F1C EuVI, 3500 rpm × 14.2 bar, SOI_e = 13° bTDC, ET = 587 µs, p_{rail} = 1800 bar, *Air* = 1393 mg/stk, x_{EGR} = 0%).

The vertical solid line represents the angular position at which $p_{inj,in}$ starts to change because of the nozzle opening (cf. the solid light blue line plotted in the upper portion of Figs. 2-4), as a result of the electric current (solid red line plotted in the upper portion of Figs. 2-5) that triggers the injector to open. The electric start of injection is an engine calibration parameter and is related to the increase in the current signal. After the nozzle opening delay has elapsed, the injection rate (dotted line plotted in the upper portion of Figs. 2-5) becomes higher than zero, thus indicating that the fuel injection has started indeed. SOI_h is virtually synchronous with the abovementioned instant that closely corresponds to the first change in $p_{inj,in}$: any delay between $p_{inj,in}$ and SOI_h should then be attributed to the time employed by the pressure wave to

propagate from the nozzle to the injector inlet. Furthermore, since the injector rate was measured separately at the hydraulic test rig for the same p_{rail} and ET conditions, any effect due to the differences between the thermal regimes at the engine and hydraulic test rig cannot be here considered and is therefore neglected. The signals $p_{inj,in}$ and injection rate are not generally available at the engine testbed and therefore the SOI_h estimation cannot be performed if only the in-cylinder pressure is acquired (without additional data at the hydraulic test rig).

Significant events linked to the combustion dynamics, which are detected by means of the MIF, have been marked with red dots in the bottom part of Figs. 2-5. In particular, SOI_h, marked with a first dot, coincides with the angular position at which $\bar{\nu}$ starts to increase from a roughly constant value, whereas the following dot, indicated as either SOC_{cool} (if a two-stage combustion process, featuring both cool and hot flames, is present, as in Figs 2-4) or SOC (if a one-stage combustion process is present, as in Fig 5), is the next local minimum of the instantaneous frequency.

The injected fuel increases the mass inside the combustion chamber with a slight influence on the corresponding p_{cyl} signal: for this reason, a small growth of $\bar{\nu}$ can be noted ~~close to~~ just after SOI_h. The high temperature, due to the engine piston compression, determines a fast vaporization of the fuel, with its latent heat of vaporization that mitigates the in-cylinder pressure rise, thus giving rise to a sudden reduction in $\bar{\nu}$. A sharp increase in $\bar{\nu}$ is then observed as soon as chemical reactions of fuel with air occur to a significant extent and an obvious minimum point is therefore reached at SOC_{cool} (or at SOC). The simple single zone analysis detects an increase from zero in the HRR and x_b diagrams for virtually the same angle.

The following local maximum point in $\bar{\nu}$ is related to the premixed combustion development and a local maximum in *HRR* is correspondingly detected. A following local minimum is found in the $\bar{\nu}$ trace if combustion is characterized by a two-stage ignition in which cool flame and hot flame events can be distinguished. This two-stage combustion, typical of the *LTC* mode (and in general of diesel conventional combustion at low loads), highlights two minima along the instantaneous frequency curve, indicated as SOC_{cool} and SOC_{hot} (cf. Figs. 2-4). Both of them, together with SOC in Fig. 5, correspond to the crank angles at which the HRR curve (cf. the dotted pink line plotted in the bottom part of Figs. 2-5) becomes positive and steeply increases, respectively.

Comparing Fig. 2 with Fig. 3, a higher p_{cyl} (blue solid line with dots in the upper part of Figs. 2-5) is detected in case of lower EGR (x_{EGR} = 41% in Fig. 3 and x_{EGR} = 55% of Fig. 2). The first-stage ignition delay (ID_{cool}) grows as *EGR* increases since EGR slows down the reactions of the fuel [44]. In fact, in Fig.2 SOC_{cool} occurs at around 352 °CA, whereas SOC_{cool} occurs at around 348 °CA in Fig. 3 (SOI_h keeps practically the same, about 341 °CA). The reactions pertaining to the hot combustion event are also related to EGR quantity and in fact SOC_{hot} occurs earlier for Fig. 3 than for Fig 2. This means that the second-stage ignition delay (ID_{hot}) augments in Fig. 2 compared to Fig. 3.

Furthermore, the HRR peak point is higher in Fig. 3 than in Fig. 2 and this highlights a more intense hot combustion, whereas the cool flames seem to be more intense in the case of Fig. 2. In general, the more intense the cool flames are, the less intense is the corresponding hot combustion and vice versa. The difference in the $\bar{\nu}$ values during the mean instantaneous frequency transition from the local minimum (located at either SOC_{cool} or SOC_{hot}) to the next local maximum is consistent with the magnitude of the corresponding HRR peaks: the higher the HRR peak, the higher the differences in the considered $\bar{\nu}$ values.

Fig. 4 refers to the same working conditions as Fig. 2 (cf. Table 2), except for a more advanced SOI, at about 28 °CA bTDC (instead of 22 °CA in Fig. 2). Again, SOI_h is detected by both a decrease in the $p_{inj,in}$ time history and a small increase in $\bar{\nu}$. The plots still show a two-stage combustion. A longer ID_{cool} is found in Fig. 4 than in Fig. 2, because the reaction of the fuel injected in a colder in-cylinder gas mixture requires more time to occur. The distance between hot ignition (start of hot flames) and cold ignition (start of cool flames), i.e. ID_{hot}, also tends to grow.

In Fig. 5, the instantaneous pressure in the pipe that joins the rail to the injector is not reported because such signal was not available for this engine. The SOI_h is located where the value of $\bar{\nu}$ starts to increase, i.e. at around 350 °CA (this value is consistent with the adopted value of SOI_e and with the typical values of nozzle opening delays measured for solenoid injectors at the hydraulic test rig under the same rail pressure). A single-stage combustion occurs because only one local minimum is detected and, consequently, this minimum is labeled as SOC; this is physically consistent since the diesel fuel passes from two-stage combustion to single-stage combustion as the pressure p_{cyl} significantly grows in Fig. 5, compared to Figs. 2-4.

For the HRR curve, a vigorous rise related to premixed combustion takes place and abruptly leads to a HRR value of nearly 30 J/°CA at around 356 °CA, which corresponds to the maximum of $\bar{\nu}$. The premixed combustion is followed by a diffusive phase that exhibits a much milder slope of the HRR curve with respect to θ. The TFA highlights this evolution of the HRR as well: first, $\bar{\nu}$ displays a sharp maximum peak point that is related to the premixed combustion while, after that, there is a subsequent gradual decrease in $\bar{\nu}$ that starts at around 358 °CA and that is related to the diffusive combustion phase.

Figures 6-11 show data of ignition delays (in μs) for the sweeps of EGR (Figs. 6, 8 and 10) and of SOI_e (Figs. 7, 9 and 11), in the case of the PCCI engine, according to the working conditions illustrated in Table 3. As the combustion in the PCCI engine always showed a two-stage development, ID_{cool} and ID_{tot} data are plotted ($ID_{tot}=ID_{cool}+ID_{hot}$).

Table 3. Engine working conditions for Figs. 6-11.

Figure	Engine	Input parameters					Measured Values		
		N [rpm]	SOI_e [°CA bTDC]	ET [µs]	p_{rail} [bar]	*Air* [mg/stk]	x_{EGR} [%]	λ [-]	*bmep* [bar]
6	F1C PCCI	1400	28	500	700	(sweep) 328÷ 474	(sweep) 43 ÷ 57	(sweep) 1.26 ÷ 1.82	3.6
7	F1C PCCI	1400	(sweep) 24 ÷ 34	500	700	328	57	1.26	3.6
8	F1C PCCI	2000	22	400	1000	(sweep) 373÷ 544	(sweep) 41 ÷ 55	(sweep) 1.42 ÷ 2.07	3.4
9	F1C PCCI	2000	(sweep) 18 ÷ 28	400	1000	373	55	1.42	3.4
10	F1C PCCI	2000	28	400	1400	(sweep) 400 ÷ 606	(sweep) 31 ÷ 50	(sweep) 1.12 ÷ 1.70	5.0
11	F1C PCCI	2000	(sweep) 24 ÷ 38	400	1400	400	50	1.12	5.0

The ignition delays were evaluated by considering the significant points revealed by the TFA (these points were marked with red dots in Figs. 2-5). By considering the injection curve obtained at the hydraulic test rig, it was also possible to estimate an ignition dwell (IDw), that can be defined as the time interval (in µs) from the end of the fuel injection to the start of the cool flame combustion [3,45]. This parameter is then positive if SOC_{cool} occurs after the end of the hydraulic injection (EOI_h), condition that is typical of PCCI combustion modes. In conventional combustion mode, instead, IDw is negative as it is clearly shown in Fig. 5. Only at low loads, the possible cool flames of a conventional combustion may

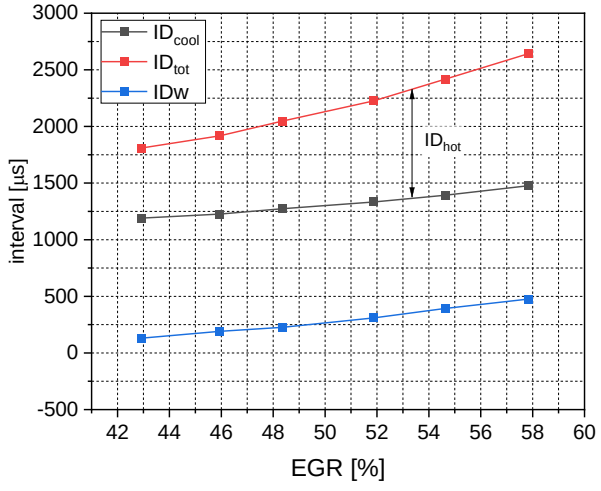

Figure 6. Evaluation of ID and IDw along an EGR sweep for the working conditions 5 in Table 3 (F1C PCCI, EGR sweep, 1400 rpm × 3.6 bar, SOI_e = 28° bTDC, ET = 500 µs, p_{rail} = 700 bar).

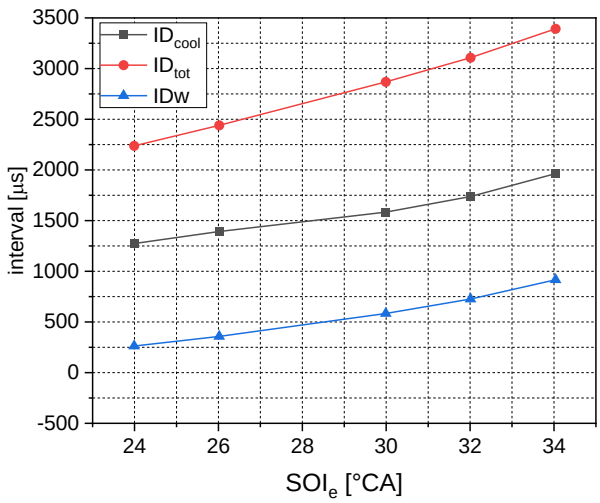

Figure 7. Evaluation of ID and IDw along a *SOI* sweep for the working conditions 6 in Table 3 (F1C PCCI, SOI_e sweep, 1400 rpm × 3.6 bar, ET = 500 µs, p_{rail} = 700 bar, *Air* = 328 mg/stk, x_{EGR} = 57%).

start before the end of the injection, with only a portion of the fuel burning under premixed combustion and the remaining portion burning under diffusive combustion.

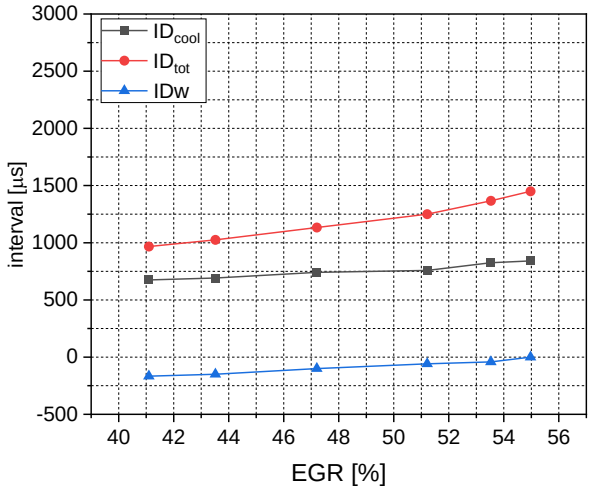

Figure 8. Evaluation of ID and IDw along an EGR sweep for the working conditions 7 in Table 3. (F1C PCCI, EGR sweep, 2000 rpm × 3.4 bar, SOI_e = 22° bTDC, ET = 400 µs, p_{rail} = = 1000 bar).

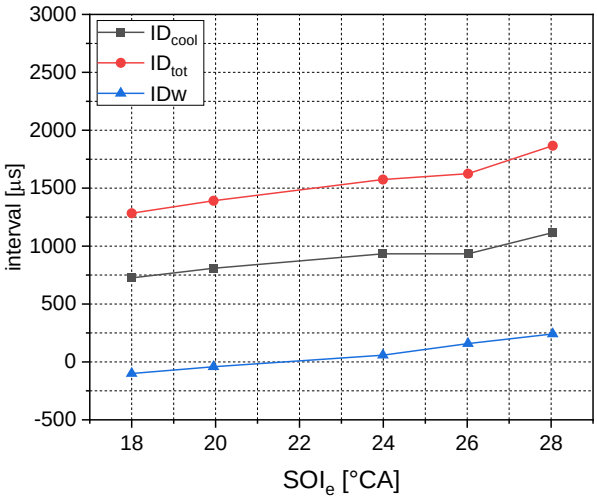

Figure 9. Evaluation of ID and IDw along a SOI sweep for the working conditions 8 in Table 3. (F1C PCCI, SOI_e sweep, 2000 rpm × 3.4 bar, ET = 400 µs, p_{rail} = 1000 bar, Air = 373 mg/stk, x_{EGR} = 55%).

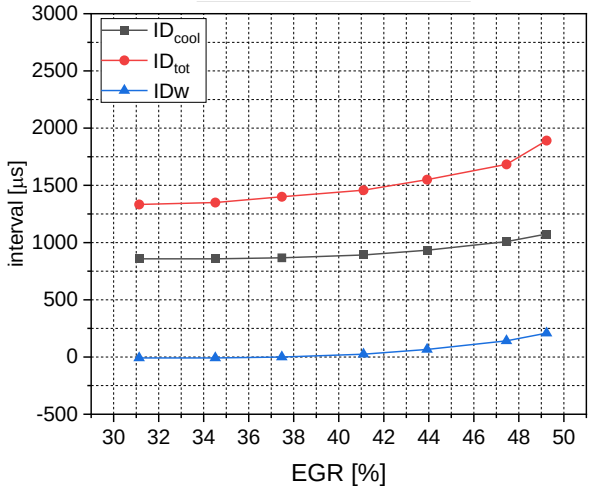

Figure 10. Evaluation of ID and IDw along an EGR sweep for the working conditions 9 in Table 3. (F1C PCCI, EGR sweep, 2000 rpm × 5 bar, SOI_e = 28° bTDC, ET = 400 µs, p_{rail} = = 1400 bar).

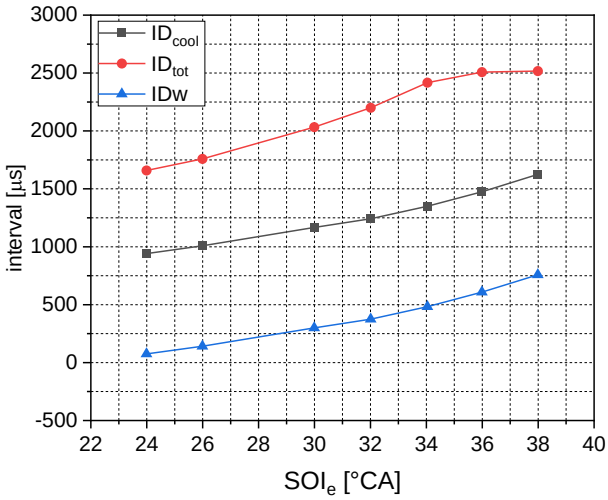

Figure 11. Evaluation of ID and IDw along a SOI sweep for the working conditions 10 in Table 3. (F1C PCCI, SOI_e sweep, 2000 rpm × 5 bar, ET = 400 µs, p_{rail} = 1400 bar, Air = 400 mg/stk, x_{EGR} = 50%).

For fixed working conditions of N, p_{rail}, ET and SOI_e, a larger EGR fraction makes both ID_{cool} and ID_{hot} increase, in line with what previously observed for Figs. 2 and 3. Similar trends are found when SOI_e occurs earlier for fixed working condition and EGR fraction (cf. Figs 10 and 11). When SOI_e is progressively increased before TDC (fuel injection is progressively advanced with respect to TDC), the fuel is injected in a progressively colder environment, taking longer to react. Therefore, the higher the SOI_e (bTDC), the higher ID_{cool}, ID_{hot} and IDw. For low EGR and SOI_e values, IDw is negative (Figs. 8-9). However, as either EGR or SOI_e increases, IDw tends to become positive (Figs. 10-11). Figs. 7, 9

and 11 show analogous results as those reported in Fig. 6, 8 and 10, but highlight a stronger effect of SOI_e than that of EGR in the variation of ID_{cool} and ID_{hot}. In other words, the first and second stage ignition delays seem to be more sensitive to SOI_e than to *EGR* for the considered engine.

Data shown in Figs. 6 and 8 have also been used to perform the analyses in Figs. 12 and 13, respectively. These figures report in red with round symbols the estimated injected mass fraction q_{inj} at SOC_{cool} (the instant at which HRR and x_b start to be different from zero) and in grey with square symbols the x_b at SOC_{hot}.

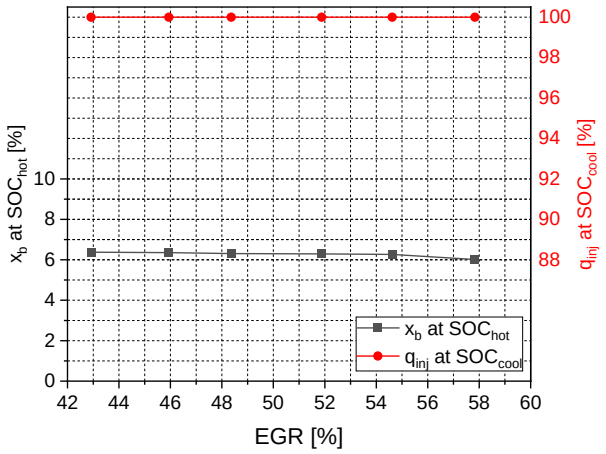

Figure 12. Injected quantity at SOC_{cool} and mass fraction burned at SOC_{hot} for the *EGR* sweep of Fig. 6 (F1C PCCI, EGR sweep, 1400 rpm × 3.6 bar, SOI_e = 28° bTDC, ET = 500 µs, p_{rail} = 700 bar).

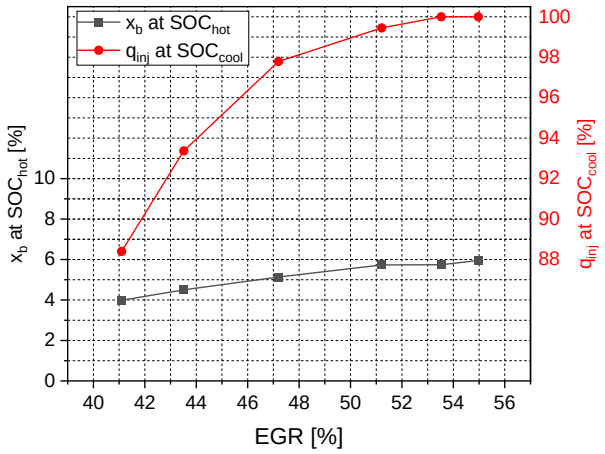

Figure 13. Injected quantity at SOC_{cool} and mass fraction burned at SOC_{hot} for the EGR sweep of Fig. 8. (F1C PCCI, EGR sweep, 2000 rpm × 3.4 bar, SOI_e = 22° bTDC, ET = 400 µs, p_{rail} = 1000 bar).

In Fig. 12, when combustion starts, all the fuel has already been injected (q_{inj} is 100% at SOC_{cool}) and therefore the corresponding IDw in Fig. 6 is always positive. The value of x_b at SOC_{hot} is affected by *EGR* to a negligible extent and this means that the quantity of fuel that burns in the cool flame is practically constant and independent of *EGR*.

The trends shown in Fig. 13 are different from those in Fig. 12: at low EGR values (or SOI_e values, although the results with respect to injection timing are not presented for the sake of conciseness) the fuel is injected in an environment that accelerate reactions. Therefore, the fuel can start to react before the end of the injection. If q_{inj} at SOC_{cool} is lower than 100%, the corresponding IDw (in Fig. 8) is negative: the lower the q_{inj} fraction at SOC_{cool}, the more negative the corresponding IDw. The value of x_b at SOC_{hot} is also influenced by q_{inj} at SOC_{cool}: for lower *EGR* (or SOI_e) values reactions are faster and the quantity of fuel that burns before the hot ignition is larger. Most of the fuel is injected before the onset of the hot combustion (at least 88% has already been injected at SOC_{cool} in Fig. 13), whereas a different situation is encountered in conventional diesel combustion, which the full load condition in Fig. 5 refers to. In this case, q_{inj} evaluated at the start of the single stage combustion is lower than 5%, as can be computed by performing an integral of the injection rate (reported in the upper part of Fig. 5) over time from t=0 up to the time instant corresponding to SOC.

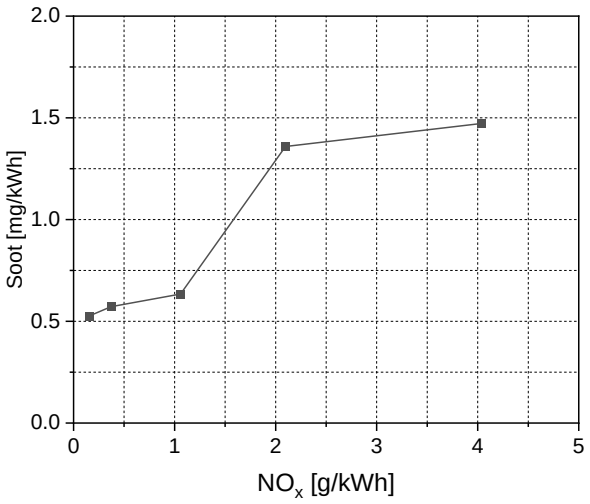

Figure 14. NO_x-soot trade-off for the EGR sweep of Fig. 6 and 12 (F1C PCCI, EGR sweep, 1400 rpm × 3.6 bar, SOI_e = 28° bTDC, ET = 500 µs, p_{rail} = 700 bar).

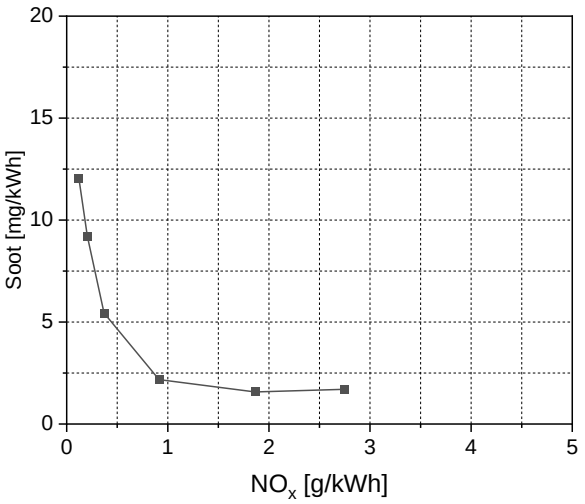

Figure 15. NO_x-soot trade-off for the EGR sweep of Fig. 8 and 13 (F1C PCCI, EGR sweep, 2000 rpm × 3.4 bar, SOI_e = 22° bTDC, ET = 400 µs, p_{rail} = 1000 bar).

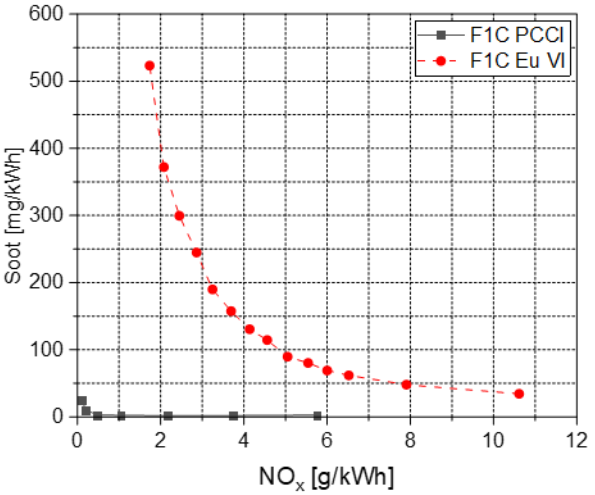

Figure 16. Comparison of an NO_x-soot trade-off between F1C PCCI and F1C Eu VI engines, at N = 2000 rpm and $bmep$ = 5 bar.

Figures 14 and 15 show engine-out soot as a function of engine-out NO_x for the same operating conditions of Figs. 12 and 13, respectively. It is worthy to note that soot emissions are a few orders of magnitude lower than NO_x, as soot is reported in terms of mg/kWh whereas NO_x is in g/kWh.

High values of SOI_e are needed to effectively exploit an early PCCI combustion, for which an increase in EGR determines a simultaneous reduction in both NO_x and soot engine-out emissions (cf. Fig. 14), whereas the NO_x-soot trade-off, which is typical of the conventional combustion, occurs in Fig. 15. In the latter case, a PCCI combustion cannot therefore be

identified, although a low temperature combustion has been obtained and in fact soot levels are much lower than typical values for conventional diesel combustion. This is proved in Fig 16, which compares the NO_x-soot trade-off obtained in the PCCI engine with a single advanced injection pattern (black solid line) to one obtained in the standard EuVI engine with a triple injection pattern (red dashed line), both evaluated at N = 2000 rpm and *bmep* around 5 bar.

On the other hand, when the soot NO_x trade-off is not present as is in the case of Fig. 14, soot emissions are anyway still lower than in Fig. 15.

5. Conclusions

The TFA has been applied to the Δp_{comb} signal for single injection strategies referring to both part loads under PCCI combustion mode and to full load under conventional combustion mode. The objective is the detection of the hydraulic SOI and of the SOC, which are the instants necessary to calculate the ignition delay. The time frequency analysis predictions are validated by means of the results of an apparent heat release rate model (for SOC detection) as well as by comparison with injection rate experimental data taken at the hydraulic test rig and with rail-to-injector pipe measurements on the engine (for SOI_h detection).

The MIF of the Δp_{comb} signal is the sensitive variable: it is roughly constant before the injection, which is highlighted by a small increase in $\overline{\nu}$, then a fast decrease in the $\overline{\nu}$ signal occurs that corresponds to the fast fuel vaporization. The subsequent local minimum corresponds to the SOC. In the case of a one-stage combustion, which is typical of conventional diesel combustion, only one minimum is detected. In the case of a two-stage combustion, which is typical of PCCI combustion modes and of conventional diesel combustion at low loads, the first minimum corresponds to the start of the cool flames and the next one corresponds to the start of the hot flames. The evaluation of these crank angles allows the calculation of ID for cool and hot flames.

Considering the experimental single-injection rate signal together with the instantaneous mean frequency it was also possible to evaluate the ignition dwell (IDw), i.e. the time interval from the end of the fuel injection to the start of combustion. The LTC and the conventional combustion modes showed different behaviors. A typical feature of PCCI combustion modes, especially those employing high EGR rates and early injection strategies, is the highly premixed combustion phase, confirmed by a positive IDw. On the contrary, conventional combustion is characterized by a negative IDw, since only a small portion of fuel has been injected at the moment of SOC: this corresponds to a low quantity of fuel burning under premixed combustion, while most of it will burn under diffusive mode.

In addition to this, the highly premixed mode shows the absence of a usual NO_x-soot trade off, which is typical of conventional combustion mode. Even in case of EGR or SOI_e that are not brought to levels able to fully exploit the

potentialities of PCCI combustion (i.e., complete absence of the NO_x-soot trade-off), low temperature combustion mode can still provide clear advantages in terms of NO_x-soot trade-off curve if compared with conventional combustion mode.

Abbreviations

bmep	brake mean effective pressure
bTDC	before top dead center
CA	crank angle (degree)
EGR	exhaust gas recirculation
ET	energizing time
FPT	Fiat Powertrain Technology
HC	unburned hydrocarbons
HRR	heat release rate
HT	high temperature
ID	ignition delay
IDw	ignition dwell
ID_{cool}	ignition delay of cool flames
ID_{hot}	ignition delay of hot flames
ID_{tot}	total ignition delay
LT	low temperature
LTC	low temperature combustion
MIF	mean instantaneous frequency
N	engine speed
NO_x	nitrogen oxides
NTC	negative-temperature coefficient
PCCI	Premixed Charge Compression Ignition
PM	Particulate Matter
p_{cyl}	in-cylinder pressure
$p_{inj,in}$	pressure at the injector inlet
p_{mot}	motored in-cylinderpressure at the injector inlet
p_{rail}	rail pressure

q_{inj}	injected mass fraction
SOC	start of combustion
SOC_{cool}	start of combustion of cool flames
SOC_{hot}	start of combustion of hot flames
SOI_e	electrical start of injection
SOI_h	hydraulic start of injection
stk	stroke
x_b	mass fraction burned
x_{EGR}	mass fraction of exhaust gas recirculation
T	temperature
TDC	top dead center
TFA	time frequency analysis
Δp_{comb}	increase in pressure due to combustion
λ	air-fuel equivalence ratio
$\bar{\nu}$	mean instantaneous frequency
θ	crank angle

Acknowledgements

The authors want to acknowledge FPT Industrial, and in particular Gilles Hardy, for providing the test engines and for the valuable technical support during the investigation.

AVL is also acknowledged for offering licence to use CONCERTO 5 within the frame of the UPP (University Partnership Program).

Author contributions

d'Ambrosio Stefano: Data curation, Visualization, Methodology, Software, Writing - Original Draft, Writing - Review & Editing. Ferrari Alessandro: Conceptualization, Methodology, Software, Writing - Original Draft, Writing - Review & Editing. Mancarella Alessandro: Investigation, Writing - Original Draft, Writing - Review & Editing.

References

[1] Heywood JB. Internal combustion engine fundamentals. McGraw-Hill Education, 2nd edition, 2018. ISBN 978-1-260-11610-6.

[2] Combustion in Diesel Engines. https://www.dieselnet.com/tech/diesel_combustion.php.

[3] Low Temperature Combustion. https://www.dieselnet.com/tech/engine_ltc.php.

[4] Aldhaidhawi M, Chiriac R, Badescu V. Ignition delay, combustion and emission characteristics of Diesel engine fueled with rapeseed biodiesel – A literature review. Renew Sustain Energy Reviews; 2007; 73:178–186. doi: 10.1016/j.rser.2017.01.129.

[5] Finesso R, Spessa E. Ignition delay prediction of multiple injections in diesel engines. Fuel 2014; 119:170-190. doi: 10.1016/j.fuel.2013.11.040.

[6] Hoang V, Thi L. Experimental study of the ignition delay of Diesel/biodiesel blends using a shock tube. Bio Systems Engineering; 2015; 134:1–7.

[7] Rothamer DA, Murphy L. Systematic study of ignition delay for jet fuels and diesel fuel in a heavy-duty diesel engine. Proc Combust Inst 2013; 34:3021-3029. doi: 10.1016/j.proci.2012.06.085.

[8] d'Ambrosio S, Gaia F, Iemmolo D, Mancarella A. et al. Performance and Emission Comparison between a Conventional Euro VI Diesel Engine and an Optimized PCCI Version and Effect of EGR Cooler Fouling on PCCI Combustion. SAE Technical Paper 2018-01-0221, 2018, doi:10.4271/2018-01-0221.

[9] Marvin CF. Combustion time in the engine cylinder and its effects on engine performance. NACA Tech Report 276; 1927.

[10] Shahabuddin M, Liaquat AM, Masjuki HH, Kalam MA, Mofijur M. Ignition delay, combustion and emission characteristics of diesel engine fueled with biodiesel. Renewable and Sustainable Energy Reviews 2013; 21:623-632. doi: 10.1016/j.rser.2013.01.019.

[11] Stone R, Introduction to Internal Combustion Engines. 4th edition, Macmillan Press Ltd, London, 2012.

[12] Piloto Rodríguez R, Sierens R, Verhelst S. Ignition delay in a palm oil and rapeseed oil biodiesel fuelled engine and predictive correlations for the ignition delay period. Fuel 2011; 90:766-772. doi:10.1016/j.fuel.2010.10.027.

[13] Assanis DN, Filipi ZS, Fiveland SB, Simiris M. A predictive ignition delay correlation under steady-state and transient operation of a direct injection diesel engine. J. Eng. Gas Turbines Power 2003; 125:450–7.

[14] Katrašnik T, Trenc F, Oprešnik SR. A New Criterion to Determine the Start of Combustion in Diesel Engines J. Eng. Gas Turbines Power – Trans. ASME; 2006; 128:928–933. doi: 10.1115/1.2179471.

[15] Bodisco T, Low Choy S, Brown RJ. A Bayesian approach to the determination of ignition delay. Applied Thermal Engineering 2013; 60:79-87. doi: 10.1016/j.applthermaleng.2013.06.048.

66:55-64. doi: 10.1016/j.applthermaleng.2014.01.066.

[16] Catania AE, Misul D, Spessa E, Vassallo A. A new quasi-dimensional multizone combustion diagnostic model for the analysis of heat-release, flame propagation parameters and nitric oxide formation in SI engines. COMODIA 2004, Yokohama, Japan; 2004.

[17] Baratta M, Catania AE, Ferrari A, Finesso R, Spessa E. Premixed-diffusive multizone model for combustion diagnostics in conventional and PCCI diesel engines. J Eng Gas Turb Power 2011;133(10):102801-1–102801-13. doi: 10.1115/1.400304.

[18] Tauzia X, Maiboom A, Shah SR. Experimental study of inlet manifold water injection on combustion and emissions of an automotive direct injection diesel engine. Energy; 2010; 35(9):3628-3639.

[19] Lata D, Misra A. Analysis of ignition delay period of a dual fuel diesel engine with hydrogen and LPG as secondary fuels. International Journal of Hydrogen Energy; 2011; 36(5):3746-3756.

[20] Lu X, Ge Y, Wu S, Han X. An Experimental Investigation on Combustion and Emissions Characteristics of Turbocharged DI Engines Fueled with Blends of Biodiesel. SAE Technical Paper 2005-01-2199; 2005.

[21] Thoo WJ, Kevric A, Ng HK, Gan S, Shayler P, La Rocca A. Characterisation of ignition delay period for a compression ignition engine operating on blended mixtures of diesel and gasoline. Applied Thermal Engineering 2014. https://doi.org/10.1016/j.applthermaleng.2014.01.066.

[22] Gatowski JA, Balles EN, Chun KM, Nelson FE, Ekchian JA, Heywood JB. Heat Release Analysis of Engine Pressure Data. SAE Technical Paper 841359; 1984. doi: 10.4271/841359.

[23] Kamimoto T, Minagawa T, Kobori K. A Two-Zone Model Analysis of Heat Release Rate in Diesel Engines. SAE Technical Paper 972959; 1997. doi: 10.4271/972959.

[24] Khaled F, Badra J, Farooq A. Ignition delay time correlation of fuel blends based on Livengood-Wu description. Fuel 2017; 209:776-786. doi: 10.1016/j.fuel.2017.07.095.

[25] Goldsborough SS. A chemical kinetically based ignition delay correlation for iso-octane covering a wide range of conditions including the NTC region. Combust Flame 2009; 156:1248-1262. doi: 10.1016/j.combustflame.2009.01.018.

[26] Hardenberg HO, Hase FW. An empirical Formula for Computing the Pressure Rise Delay of a Fuel from its Cetane Number and from the Relevant Parameter of Direct Injection Diesel Engines. SAE Technical Paper 790493; 1979. doi: 10.4271/790493

[27] Kadota T, Hiroyasu H, Oya H. Spontaneous Ignition Delay of Fuel Droplet in High Pressure and High Temperature Gaseous Environments. Bullettin of the JSME; April 1996, 19(130):437–445.

[28] Pan J, Zhao P, Law CK, Wei H, A predictive Livengood–Wu correlation for two-stage ignition, Int J Engine Res 2016;17(8):825–35. doi: 10.1177/1468087415619516.

[29] Blomberg CK, Mitakos D, Bardi M, Boulouchos K, Wright YM, Vandersickel A. Extension of the Phenomenological 3-Arrhenius Auto-Ignition Model for Six Surrogate Automotive Fuels, SAE Technical Paper 2016-01-0755, 2016, doi: 10.4271/2016-01-0755.

[30] Zhang P,Ji W, He T, He X, Wang Z, Yang B, Law CK. First-stage ignition delay in the negative temperature coefficient behavior: Experiment and simulation. Combust Flame 2016; 167:14-23. doi: 10.1016/j.combustflame.2016.03.002.

[31] Payri R, Viera JP, Pei Y, Som S. Experimental and numerical study of lift-off length and ignition delay of a two-component diesel surrogate, Fuel 158 (2015) 957–967. doi: 10.1016/j.fuel.2014.11.072.

[32] Lillo PM, Pickett LM, Pearson H, Andersson O, Kook S. Diesel spray ignition detection and spatial/temporal correction. SAE paper 2012-01-1239; 2012.

[33] Higgins B, Siebers D, Aradi A. Diesel-spray ignition and premixed-burn behavior. In: SAE technical paper 2000-01-0940; 2000. doi: 10.4271/2000-01-0940.

[34] Fu X, Aggarwal SK. Two-stage ignition and NTC phenomenon in diesel engines. Fuel 2015; 144:188-196. doi:10.1016/j.fuel.2014.12.059.

[35] Thangaraja J, Kannan C. Effect of exhaust gas recirculation on advanced diesel combustion and alternate fuels - A review. Applied Energy 180 (2016) 169–184. doi: 10.1016/j.apenergy.2016.07.096.

[36] Kuwahara K, Tada T, Furutani M, Sakai Y, Ando H, Chemical kinetics study on two-stage main heat release in ignition process of highly diluted mixtures, SAE Int. J. Engines 6 (2013) 520–532.

[37] Shibata G, Oyama K, Urushihara T, Nakano T, The effect of fuel properties on low and high temperature heat release and resulting performance of an HCCI engine, 2004 SAE World Congress (2004) 2004-01-0553.

[38] d'Ambrosio S, Finesso R, Lezhong F, Mittica A, Spessa, E, "A control-oriented real-time semi-empirical model for the prediction of NOx emissions in diesel engines", Appl. Energy 2014, 130, 265–279. doi: 10.1016/j.apenergy.2014.05.046.

[39] Ferrari A and Mittica A, 2016, "Response of different injector typologies to dwell time variations and a hydraulic analysis of closely-coupled and continuous rate shaping injection schedules", Elsevier Press, Applied Energy 2016; 169:899-911 - ISSN 0306-2619. doi: 10.1016/j.apenergy.2016.01.120.

[40] Ferrari A and Mittica A, 2013, "Thermodynamic formulation of the constitutive equations for solids and fluids", Elsevier Press, Energy Convers Manage 2012, 66:77-86 - ISSN 0196-8904. doi: 10.1016/j.enconman.2012.09.028.

[41] Ferrari A, Manno M and Mittica A, 2008, "Cavitation Analogy to Gasdynamic Shocks: Model Conservativeness Effects on the Simulation of Transient Flows in High-Pressure Pipelines", ASME Transactions, Journal of Fluids Engineering, vol. 130:031304:1-14 - ISSN 0098-2202. doi: 10.1115/1.2842226.

[42] d'Ambrosio S, Ferrari A. Potential of double pilot injection strategies optimized with the design of experiments procedure to improve diesel engine emissions and performance. Applied Energy 2015; 155:918–932. doi: 10.1016/j.apenergy.2015.06.050.

[43] d'Ambrosio S, Ferrari A, Galleani L. In-cylinder pressure-based direct techniques and time frequency analysis for combustion diagnostics in IC engines. Energy Convers Manage 2015; 99:299–312. doi: 10.1016/j.enconman.2015.03.080.

[44] d'Ambrosio S, Ferrari A. Effects of exhaust gas recirculation in diesel engines featuring late PCCI type combustion strategies. Energy Conversion and Management 2015; 105:1269–1280. doi: 10.1016/j.enconman.2015.08.001.

[45] Musculus MPB, Miles PC, Pickett LM. Conceptual models for partially premixed low-temperature diesel combustion, Progress in Energy and Combustion Science 2013; 39:246-283. doi: 10.1016/j.pecs.2012.09.001.